

The MOLLER Experiment
An Ultra-precise Measurement of the
Weak Mixing Angle using
Møller Scattering

Update submitted to PAC 37

DRAFT

November 30, 2010

Abstract

The upgraded 11 GeV CEBAF polarized electron beam presents a compelling opportunity to measure a weak neutral current amplitude to unprecedented precision at $Q^2 \ll M_Z^2$. The result would yield a precise measurement of the weak mixing angle $\sin^2 \theta_W$, a fundamental parameter of the electroweak theory. The experimental goal of $\delta(\sin^2 \theta_W) \sim 0.1\%$, matching the accuracy of the two single best measurements by e^+e^- colliders at the Z resonance, would be accomplished by a precise measurement of the parity-violating asymmetry in fixed-target Møller scattering. The quantitative goals, the measurement strategy, and the major parameters of the experimental design in the original proposal remain unchanged, and we will refer to it frequently in this document. The original proposal document can be found at

http://hallaweb.jlab.org/12GeV/Moller/moller_final.pdf.

After presenting a brief overview of the experiment, we address a few aspects of the experimental design that have seen progress in recent months, both due to dedicated studies as well as due to technical accomplishments in other related projects. We conclude with a projection of the required beam time to achieve the proposed accuracy for the measurement.

J. Benesch, P. Brindza, R.D. Carlini, J-P. Chen, E. Chudakov, S. Covrig, C.W. de Jager,
A. Deur, D. Gaskell, J. Gomez, D.W. Higinbotham, J. LeRose, D. Mack, R. Michaels,
B. Moffit, S. Nanda, G.R. Smith, R. Suleiman, B. Wojtsekhowski

Jefferson Lab

H. Baghdasaryan, G. Cates, D. Crabb, D. Day, M.M. Dalton, C. Hanretty,
N. Kalantarians, N. Liyanage, V.V. Nelyubin, B. Norum, K. Paschke, M. Shabestari,
J. Singh, A. Tobias, K. Wang, X. Zheng

University of Virginia

S. Johnston, K.S. Kumar [Contact*], J. Mammei, L. Mercado, R. Miskimen, S. Riordan,
J. Wexler

University of Massachusetts, Amherst

J. Birchall, M.T.W. Gericke, W.R. Falk, L. Lee, S.A. Page, W.T.H. van Oers

University of Manitoba

V. Bellini, A. Giusa, F. Mammoliti, G. Russo, M.L. Sperduto, C.M. Sutura

INFN Sezione di Catania and Universita' di Catania

D.S. Armstrong, T.D. Averett, W. Deconinck, J. Katich, J.P. Leckey

College of William & Mary

K. Grimm, K. Johnston, N. Simicevic, S. Wells

Louisiana Tech University

L. El Fassi, R. Gilman, G. Kumbartzki, R. Ransome,

Rutgers University

J. Arrington, K. Hafidi, P.E. Reimer, P. Solvignon

Argonne National Lab

P. Cole, D. Dale, T.A. Forest, D. McNulty

Idhao State University

E. Fuchey, F. Itard, C. Muñoz Camacho

LPC Clermont, Université Blaise Pascal

E. Cisbani, S. Frullani, F. Garibaldi

INFN Gruppo Collegato Sanita' and Istituto Superiore di Sanita'

R. De Leo, L. Lagamba, S. Marrone

INFN, Sezione di Bari and University di Bari

F. Meddi, G.M. Urciuoli

Dipartimento di Fisica dell'Universita' la Sapienza and INFN Sezione di Roma

R. Holmes, P. Souder

Syracuse University

G. Franklin, B. Quinn

Carnegie Mellon University

N. Morgan, M. Pitt

Virginia Polytechnic Institute and State University

P.M. King, J. Roche
Ohio University

J.A. Dunne, D. Dutta
Mississippi State University

A.T. Katramatou, G. G. Petratos
Kent State University

A. Ahmidouch, S. Danagoulian
North Carolina A&T State University

S. Kowalski, V. Sulkosky
MIT

P. Decowski
Smith College

J. Erler
Universidad Autónoma de México

M.J. Ramsey-Musolf
University of Wisconsin, Madison

Yu.G. Kolomensky
University of California, Berkeley

K. A. Aniol
California State U. (Los Angeles)

C.A. Davis, W.D. Ramsay
TRIUMF

J.W. Martin
University of Winnipeg

E. Korkmaz
University of Northern British Columbia

T. Holmstrom
Longwood University

S.F. Pate
New Mexico State University

G. Ron
Hebrew University of Jerusalem

D.T. Spayde
Hendrix College

P. Markowitz
Florida International University

F.R. Wesselmann
Xavier University of Louisiana

F. Maas
Johannes Gutenberg Universitaet Mainz

C. Hyde
Old Dominion University

F. Benmokhtar
Christopher Newport University

E. Schulte
Temple University

C. Hyde
Old Dominion University

M. Capogni
*Istituto Nazionale di Metrologia delle Radiazioni Ionizzanti ENEA and INFN Gruppo
Collegato Sanita'*

R. Perrino
INFN Sezione di Lecce

*kkumar@physics.umass.edu

Contents

1	Introduction and Motivation	3
1.1	Physics Motivation Summary	4
2	Experimental Design Update	5
2.1	Design Overview	6
2.1.1	Polarized Beam	6
2.1.2	Liquid Hydrogen Target	6
2.1.3	Spectrometer System	7
2.1.4	Integrating Detectors	7
2.1.5	Tracking Detectors	8
2.2	Backgrounds Update	9
2.2.1	Inelastic e-p Scattering	9
2.2.2	Pions from Weak Decays	9
2.3	Polarimetry	10
3	Director’s Review	11
4	Beamtime Request	12
4.1	The Three Runs	13
4.1.1	Run I	13
4.1.2	Run II	13
4.1.3	Run III	13
4.2	Special Beam Considerations	14
4.2.1	Wien Angle “Tweaks”	14
4.2.2	Transverse Polarization Running	14
4.2.3	The Double-Wien	15
4.2.4	Beam Energy	15
A	Liquid Hydrogen Target Update	16
B	Spectrometer Design	19
B.1	Spectrometer	19
B.2	Verifying the Proposal Field	20

<i>CONTENTS</i>	2
B.3 Towards a More Realistic Magnet Design	22
B.4 Engineering Review	26
B.5 Optimizing for Physics Considerations	28
C Backgrounds Update	32
C.1 Correction from Inelastic e-p Scattering	32
C.2 Pions from Weak Decays	34
D Tracking System	36
D.1 Tracking	36
D.1.1 Backgrounds and Spectrometer Optics	36
D.1.2 Effective Kinematics	39
D.1.3 Conceptual Design	40
D.1.4 Focal Plane Scanner	40

Chapter 1

Introduction and Motivation

Since the $SU(2)_L \times U(1)_Y$ gauge theory of electroweak interactions was established more than three decades ago as a cornerstone of the Standard Model, experiments have been searching for clues to address the model's many shortcomings. Compelling theoretical arguments point to pursuing measurements that are sensitive to various kinds of new dynamics at the TeV scale in two broad thrusts: hadron and lepton colliders at the highest possible center of mass energies on the one hand, and targeted precision electroweak measurements at low energy on the other.

One class of accelerator-based low energy measurements focus on electroweak observables that can be calculated with high accuracy and aim to achieve sufficient precision so that indirect effects of new dynamics at the TeV scale might become manifest. In this document, we update the status of the MOLLER project (proposal E09-005), a new electroweak measurement that can potentially be the most sensitive such low energy measurement, at least as far as flavor-diagonal neutral current interactions are concerned.

We propose to measure the parity-violating asymmetry A_{PV} in the scattering of longitudinally polarized 11 GeV electrons from the atomic electrons in a liquid hydrogen target (Møller scattering). In the Standard Model, A_{PV} is due to the interference between the electromagnetic amplitude and the weak neutral current amplitude, the latter being mediated by the Z^0 boson. A_{PV} is predicted to be 35.6 parts per billion (ppb) at our kinematics. Our goal is to measure A_{PV} to a precision of 0.73 ppb. The result would yield a measurement of the weak charge of the electron Q_W^e to a fractional accuracy of 2.3% at an average Q^2 of 0.0056 (GeV/c)^2 .

Within the context of the Standard Model, the Q_W^e measurement yields a determination of the weak mixing angle $\sin^2 \theta_W$ with an uncertainty of $\pm 0.00026(\text{stat}) \pm 0.00013(\text{syst})$, similar to the accuracy of the single best such determination from high energy colliders. Thus, our result could potentially influence the central value of this fundamental electroweak parameter, a critical input to deciphering signals of any physics beyond the Standard Model that might be observed at the Large Hadron Collider (LHC).

1.1 Physics Motivation Summary

A model-independent way to quantify the sensitivity of a low energy electroweak measurement is in the context of 4-Fermi contact interactions, as described in Sec. 1.4 of the proposal (Eqn 1.4). The proposed accuracy of the measurement provides access to an energy scale of 7.5 TeV (Eqn 1.5), better than the sensitivity of any previous measurement of a flavor-diagonal amplitude at fixed target or at colliders.

Within any new physics scenario, such as Supersymmetry models or models with new massive Z' bosons, the 7.5 TeV limit can be converted to a model-dependent limit on specific of physics amplitudes involving electrons in the initial and final state. Such limits will take on added significance should any new physics anomalies be discovered at the Tevatron or the LHC. It is likely that low energy measurements will become a necessary ingredient in unfolding the nature of the new dynamics that might be directly observed in high energy collisions. The original proposal referred to extensive literature on this issue; here we point out two new publications that reflect the growing interest of the potential measurement in phenomenological analyses of future LHC and low energy precision data [1, 2].

As described in Sec. 1.3 of the proposal, the proposed measurement will be significant even in the case that the Tevatron or LHC validates the minimal Standard Model with the discovery of a low mass Higgs boson. The prediction of a Higgs boson in range 110-160 GeV is based on an electroweak global fit of precision low energy data. However, the two most precise inputs to the fit are measurements of $\sin^2 \theta_W$ that disagree with each other by more than 3 standard deviations. Taken at face value, each measurement implies very different values for the mass of the Higgs boson. The proposed measurement of Q_W^e , given that it is designed to have an accuracy comparable to the above-mentioned measurements, will become a significant new input in future precision analyses of the internal consistency of the electroweak theory.

In summary, the proposed measurement will have a significant impact on electroweak physics in the timescale of 5 to 10 years, within a variety of outcomes of other precision measurements at high energy as well as low energy experiments. It will be a particularly robust input since it is a unique purely leptonic reaction at $Q^2 \ll M_Z^2$ with little theoretical uncertainty, and unlikely to be superceded by any other measurement proposed for new facilities in the coming decade.

Chapter 2

Experimental Design Update

The conceptual design of the experimental apparatus was described in Chapter 2 of the original proposal document, with additional details provided in a series of appendices. The design chapter followed up in Chapter 3 with a detailed discussion of potential systematic errors and the proposed strategies to control them. In this document, we focus on aspects of the design that have developed since the original proposal document was written. We once again relegate details to a new set of appendices. A recent CAD rendition of the apparatus is shown in Fig. 2.1.

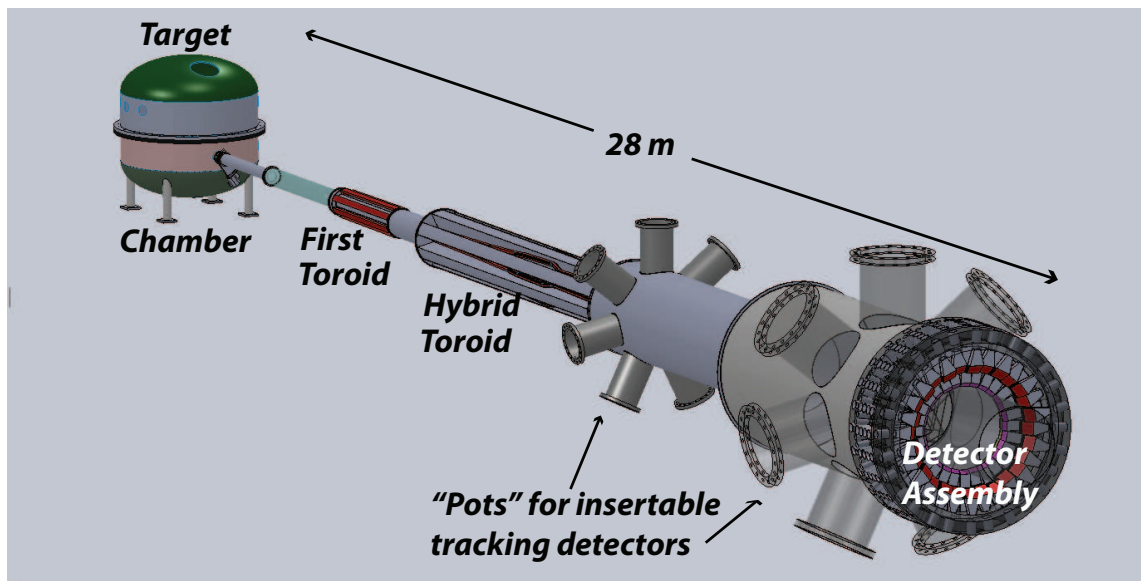


Figure 2.1: *Schematic Overview of the Experimental Apparatus.*

2.1 Design Overview

2.1.1 Polarized Beam

The preparation and control of the polarized electron beam is obviously a critical component of the apparatus and has been dealt with in detail in the original proposal (Secs 2.1, 3.1 and App. A). Our collaboration continues to gain experience in beam operation during data collection of the PREX and Qweak experiments. In collaboration with the JLab Electron Gun Group (EGG), we are learning to achieve consistently better control of beam helicity correlations at the target. In the process, incremental improvements are being accomplished towards the challenging beam parameters required for MOLLER, which are spelled out in App. A of the proposal document. For example, just before the PREX experiment, helicity-correlated laser spot-size asymmetries were measured for the first time in the JLab polarized source. The results showed that spot-size effects on the laser spot were controlled at the desired level of about 10^{-4} .

For multiple reasons, MOLLER proposes to flip the beam helicity at a rate of 2 kHz; Qweak is currently successful taking data with a 1 kHz flip rate. However, it has proven difficult to push the transition of the Pockels cell to be shorter than 60 μ s, and to keep the cell optical properties stable after the shock of the fast transitions. Although carefully tuning the HV pulse sent to the cell may reduce the problem, it now appears unlikely that the KD*P cell, as it is presently used at JLab, will be sufficient for the MOLLER experiment, unless we are willing to accept a dead time loss of 12%. The collaboration is exploring other options, including the use of RTP Pockels cells (which are not piezoelectric and therefore do not experience mechanical shock on transition), and Kerr cells.

2.1.2 Liquid Hydrogen Target

The electron beam will impinge on a 150 cm long liquid hydrogen target, dissipating ~ 5 kW to generate the required signal rate of ~ 150 GHz. Even with a 2 kHz flip rate, one of the many technical challenges will be to control target density fluctuations to be small compared to the statistical fluctuations (~ 80 ppm). The success of the target design is predicated on several novel ideas which are being tested for the first time with the Qweak design and operational experience. In addition, the cooling power needed for MOLLER has been carefully considered and the required solutions are being incorporated into the lab's planning. These considerations are discussed in detail in App. A of this document. The main conclusion is that the technical risk associated with the target and related cryogenic systems has been greatly mitigated since the proposal document was written.

2.1.3 Spectrometer System

Another technically challenging aspect of the experiment is the spectrometer and collimator system that will spatially separate Møller-scattered electrons from background. As described in detail in the original proposal (Sec. 2.3-4, App. B), the heart of the experiment is a set of two warm toroidal magnets systems, consisting of seven coils each. Over the past year, our focus has been on validating the spectrometer design and addressing the technical challenges to achieve realistic engineering designs. A Magnet Advisory Committee was formed to advise the collaboration on the technical feasibility and to move us towards solutions that would lead to ease of fabrication. The committee members are: George Clark (TRIUMF), Ernie Ihloff (MIT-Bates), Vladimir Kashikhin (Fermilab), Jim Kelsey (MIT-Bates), Dieter Walz (SLAC) and Robin Wines (JLab)

We present here a summary of recent accomplishments and future plans. The details can be found in App B of this document.

1. The TOSCA package was used to verify the proposal model for the 3-D field map of the hybrid toroid. The two field maps matched in great detail and gave very similar results in GEANT4 simulations of signal and background rates.
2. A first-pass realistic model of the hybrid toroid coil using actual conductors was made and presented to the Magnet Advisory Committee. The committee members concurred that there were no show-stoppers and made many suggestions for improvements
3. A new design incorporating these suggestions has recently been completed and is being reviewed by JLab technical staff for the first attempts at designs for structural support and water cooling.
4. The latest design has somewhat degraded performance for background rejection and “optics tweaks” are being pursued to regain the performance of the proposal field map.
5. The final tweaks must incorporate a detailed model for collimation and shielding from neutral background and so this effort will now be launched in parallel.

2.1.4 Integrating Detectors

We have taken a first pass at laying out the quartz and light guides in a CAD program. The goal is to develop sufficient detail so that engineers and designers can evaluate the complexity of the mechanical assembly. In the process a framework for realistic background simulations will also be developed. Figure 2.2 shows two views of the integrating detector layout. In this model, the air light guides are perpendicular to the charged particle trajectories, which leads to a relatively simpler

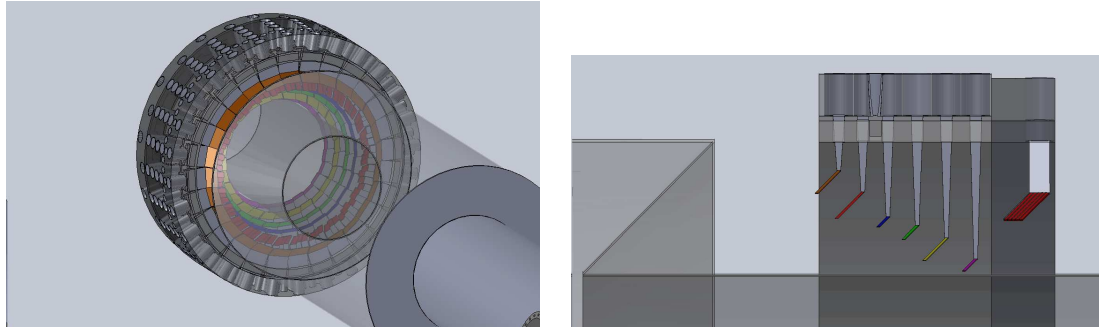


Figure 2.2: A perspective view of the integrating detector assembly is shown on the left. On the right is shown a plan cutaway view. Note that two back-to-back detectors (thin quartz and quartz/tungsten sandwich) will simultaneously measure the flux of the Møller peak.

mechanical assembly. Also shown is a new “shower-max” quartz/tungsten sandwich detector that will provide a second independent measurement of the flux in the main Møller “peak”. This detector will be less sensitive to soft photon and charged hadron backgrounds.

The detectors have been set in six radial bins that have been optimized to measure the main Møller scattering asymmetry as well as the asymmetries in the background processes of elastic and inelastic scattering from target protons. A discussion of this optimization can be found in Sec. 2.2. We are also investigating a mechanical assembly model with light guides that are parallel to the Cherenkov photons, i.e. at 45° to the charged particles. Ultimately, the most important criterion is the efficiency of delivering photons to the photocathode, so the final decision will be based on a detailed Monte Carlo study comparing the two light guide designs.

2.1.5 Tracking Detectors

We have made some progress in defining the parameters of a charged-particle tracking system which will be used to verify the spectrometer optics, measure the absolute value of Q^2 , and study backgrounds. The basic concept is to have three planes of trackers downstream of the two toroids. Two of these planes would be in the drift region in the vacuum space, as shown in Fig. 2.1. A third plane would be in air right after the charged particles exit from the angled vacuum window (see Fig. 2.2) and before the quartz detectors. This space could also hold a scanning device for a quick check of the spectrometer tune. These considerations are discussed in detail in App. D.

2.2 Backgrounds Update

A detailed discussion of backgrounds, their suppression, and potential systematic errors were discussed in Sec. 3.5 of the original document. Here we expand on two potential sources of backgrounds that will cause negligible dilution but might still require significant systematic corrections, expanding on discussions in Secs. 3.5.2 and 3.5.3.

2.2.1 Inelastic e-p Scattering

There is a small ($\sim 0.5\%$) dilution from electrons that arrive in the vicinity of the Møller peak after having scattered inelastically off protons. As discussed in the proposal, the parity-violating asymmetry in inelastic scattering involves unknown vector couplings which can potentially be significantly bigger than the weak vector charge of the proton. We have done a preliminary study of the optimization of the radial segmentation of the integrating detectors so that we will be able to measure the relevant combination of vector couplings so as to make a reliable correction to the raw Møller asymmetry.

In Fig. 2.2, the quartz is color-coded. The Møller electrons hit the red quartz while the elastic e-p electrons predominantly hit the yellow quartz. The two detectors in between (green and blue) are the relevant ones that will yield the measurements to be used to make a reliable correction. The considerations that are relevant for this analysis are discussed in App. C, and a careful analysis validates our estimate in the proposal for the systematic error in the correction.

2.2.2 Pions from Weak Decays

A challenging background to monitor and correct for is a fractionally tiny flux of pions or muons from weak decays of heavy hadrons produced by electro- or photo-production in the target. If there is sufficient polarization transfer, the potentially large analyzing power in weak decays might lead to a sizable correction. This was discussed briefly in Sec. 3.5.3 in the original proposal, where we proposed to monitor the size of such an effect by deploying a “pion” detector downstream of the primary integrating detectors.

The Director’s Review committee (see Sec. 3) shared our concerns for improving our estimates for such a background correction. They also suggested that we start thinking about contingency plans should the background asymmetry be significantly higher than anticipated. We have launched a comprehensive study of hadron electro- and photo-production. A more careful estimate of the background since the review validates the conservative upper limit of a 0.5 ppb correction assumed in the proposal document. The details of this, as well as our future plans, are described in App. C.

2.3 Polarimetry

In order to reach a robust 0.4% accuracy in beam polarimetry, we have proposed to develop two separate, continuous polarimeters for the current proposal: one based on Compton scattering from polarized laser light and the other on Moller scattering from trapped atomic hydrogen. Plans for these systems are described in the original proposal, in App. F and G.

Recent activity with Compton polarimetry at Jefferson Lab has largely focussed on the challenge of achieving high-precision at low beam energies (~ 1 GeV). The Hall A polarimeter was upgraded to use a green laser cavity as the photon target. The change in photon energy provides a higher scattering asymmetry and higher scattered photon energies which are essential for low energy operation, and will be helpful at higher energies. A new Compton polarimeter has been constructed in Hall C, and is presently being commissioned.

The collaboration is considering new design concepts for the laser system to be used at 12 GeV. One of the largest challenges to operating the JLab Compton polarimeters has been bremsstrahlung photons scattering from narrow beam apertures, which are required by the small electron-laser crossing angle. At 12 GeV, beam emittance growth driven by synchrotron radiation in the arcs of the higher passes might exacerbate this problem, and force a re-engineering of the Compton interaction region. In order to maintain high luminosity at a larger electron-photon crossing angle (and therefore larger beam apertures), a concept for a new laser system has been proposed. This concept is based on a mode-locked Fabry-Perot cavity storing coherently-pumped “bunches” of laser power. The collaboration is also evaluating other options for the laser system that will maintain sufficient statistical power while increasing electron beam apertures.

Chapter 3

Director's Review

A Director's review of the MOLLER experiment was held on January 14-15, 2010. The review was chaired by Charles Prescott (SLAC) and the other members of the committee were Doug Beck (UIUC), Dave Hertzog (UIUC), Bob Kephart (Fermilab), Bill Marciano (BNL), Matt Poelker (JLab), Michael Schmitt (Northwestern), Glenn Young (JLab) and John Weisend (SLAC). The committee reviewed the scientific relevance of the project and focussed on technical issues with the intention of establishing feasibility and impact on JLab. The full report is available [3], along with the detailed presentations by collaboration members [4].

We highlight some important quotes from the report. The primary recommendation was as follows: **The Review Committee unanimously recommends that the Director undertake planning for MOLLER now, to be ready for the 12 GeV Upgrade era.** The report also endorsed the motivation for the experiment: *Thus MOLLER, by exploiting the best qualities of the Jefferson Lab electron beam, brings new information to bear on, and to constrain interpretations of, any new physics that may result at the LHC and elsewhere.* The committee provided an endorsement of the technical feasibility of the proposed design: *The Committee could find no technical reasons the goals of MOLLER could not be reached.*

The committee report also contains a number of detailed suggestions. The need to involve engineers in the design of the spectrometer and the need for the collaboration to make early progress on its technical design was stressed. The report also pointed out the need for a careful study of the cryogenic needs of the project by JLab. The need for a detailed R&D plan, especially to achieve the challenging goals for systematic control, and a more careful study of potentially large background corrections from rare charged current processes was also pointed out. There has been progress on all these fronts, as has been highlighted in the previous chapter and the associated documentation.

Chapter 4

Beamtime Request

While the MOLLER apparatus is being designed for a beam current of $85 \mu\text{A}$ at 11 GeV, we have assumed a beam current of $75 \mu\text{A}$ and a beam polarization of 80% to formulate the beam time request. If higher beam current and/or higher beam polarization become available, the request can correspondingly be reduced using the appropriate P^2I factor. In order to ensure the technical success of this challenging measurement, we are proposing to take data in three separate run periods. These run periods have been optimized so that not only important technical milestones are met, but also that each run will provide publishable results and will significantly add to our knowledge of electroweak physics to date.

One important criterion for gauging the amount of running time required is to estimate how close one can approach counting statistics in the instantaneous raw asymmetry measurement. From our Monte Carlo simulation, we estimate that pure counting statistics for a 1 kHz pulse-pair is 83 ppm. Considering the various sources of additional fluctuations such as target density and electronics noise, an aggressive but realistic goal for final production running is 90 ppm. However, it will be challenging to achieve the final goal for the width in early running, so we will assume 100, 95 and 90 ppm respectively for the three running periods.

Another important criterion is overall efficiency. Generally, once parity experiments have been properly commissioned, the up-time should be 90% for the experimental apparatus, since stable run conditions are required over extended periods of time. Coupled with an accelerator efficiency of 70%, the final running should yield an effective efficiency greater than 60%. Again however, we are unlikely to achieve this in the early going. So, we have assumed total efficiencies of 40, 50 and 60% respectively for the three running periods.

We summarize our estimated beam time in the Table 4.1. We follow it up with a few comments about the goals of each run and certain special considerations that must be part of the discussion with both the scheduling committee and accelerator operations planning before final beam time allocation.

Run Period	1kHz Width (ppm)	% Stat. Error	Stat. (ppb)	PAC Days	Eff. %	Calendar Weeks	Comm. Weeks	Total Weeks
I	100	11.0	2.88	14	40	5	5	10
II	95	4.04	1.05	95	50	27	3	30
III	90	2.43	0.63	235	60	56	4	60
		2.05	0.53	344				100

Table 4.1: *Summary of the Estimated Beam Time ($75 \mu A$, $P_e = 80\%$).*

4.1 The Three Runs

4.1.1 Run I

The primary goal of the first run will be to commission the principal subsystems of the apparatus. The focus will be on validating the target design, the spectrometer optics, rejection of background and the demonstration that detector fluctuations are dominated by statistics. Once this is established, a reasonable goal would be to achieve a statistical error better than or equal to the E158 result, which we conservatively estimate can be done in 5 calendar weeks. The duration of production running also allows enough sensitivity to demonstrate that there are no anomalously large background asymmetries from charged current processes.

4.1.2 Run II

The primary goal of the second run is to get more than 25% of the proposed statistics so that one is able to achieve $\delta(\sin^2 \theta_W) \sim 0.0005$. This would be the single-best such measurement at $Q^2 \ll M_Z^2$, which could already potentially have a major impact on TeV-scale physics depending on the status of LHC data anomalies. The control of beam helicity correlations must be fully commissioned to achieve $\delta(A_{raw}) \sim 1$ ppb. The fractional statistical error of 4% will require modest but not the ultimate systematic control of absolute normalization errors such as the beam polarization. We have assigned 3 weeks for recommissioning of the apparatus. We will also strive to achieve better than 50% overall efficiency for data collection.

4.1.3 Run III

This run must have all aspects of the apparatus to be working to its full scope. We must also have enough diagnostics in place and sufficient trained personnel within the collaboration so that high quality data can be collected with the best possible efficiency. We are targeting 60% total efficiency. The full control of normalization errors such as the absolute value of Q^2 and the beam polarization at the level of

0.4-0.5% must be achievable. The long duration of this run likely means that it must be split between two fiscal running cycles, and we have assigned 2 weeks of commissioning for each period.

4.2 Special Beam Considerations

Systematic control is one of the most important considerations that must govern various decisions on the design as well as running conditions for the experiment. Two important aspects of this are the methods of “slow helicity reversals” (passive sign flips of the raw asymmetry), and controlled changes to the degree of transverse beam polarization.

4.2.1 Wien Angle “Tweaks”

The vector analyzing power A_T for Møller scattering at our kinematics can be as large as 14 ppm. As discussed in Sec. 3.3 of the original proposal, in order to ensure a negligible systematic error at the fraction of a ppb level due to a coupling between residual transverse components of the electron beam polarization with azimuthal imperfections in the apparatus, it will be required to make periodic corrections to the polarization launch angle at the polarized source. We estimate that changes at the level of 1° to the launch angle might be requested once a day during production running. Assuming the launch angle was set correctly given the sensitivity of the available diagnostics, over many days the total change to the launch angle should average out to zero to high precision. We expect that these changes will be small enough to have no impact on the average longitudinal polarization that will be seen in any of the Halls that happen to be running at the same time.

4.2.2 Transverse Polarization Running

The large A_T value also presents a unique opportunity to test the complete apparatus and its capability for absolute normalization at the fraction of a percent level, including detector acceptance, background corrections, azimuthal imperfections, radiative corrections, absolute value of Q^2 and the longitudinal beam polarization. This is because A_T is known theoretically at the 0.1% level. The Møller apparatus is capable of measuring A_T with a fractional statistical error of $\sim 0.2\%$ in a matter of 4 to 8 hours at full luminosity. We are therefore planning to request several periods, each lasting 2 to 3 shifts, of 100% transverse polarization in Hall A for a sensitive test of systematics. The periods can likely be synchronized with a change of beam energy that we also plan to request (see Sec. 4.2.4 below).

4.2.3 The Double-Wien

The “Double-Wien” filter at the front end of CEBAF was commissioned during the PREX run. The system accomplishes a full flip of the beam polarization direction with a aid of two Wien filters and a solenoid lens. The method is very effective because the flip is achieved with a relatively minor change to the beam optics at the front end of the machine. This is a very powerful and crucial way to cancel subtle systematic errors. It would be good to get 50 to 100 flips by this method over the duration of the full set of runs. This might require a configuration change once every 5 to 7 days during production running.

4.2.4 Beam Energy

Over the next two years, as the detailed design of the MOLLER apparatus evolves and depending on discussions with the Accelerator Division, the exact beam energy for MOLLER (somewhere in the range of 10.5 to 11 GeV) will be chosen and used to fix the geometry of the spectrometer and the associate collimation. Once this energy is chosen, we will immediately investigate what minimum configuration change would accomplish a beam polarization sign flip either by slightly reducing the total energy of the machine or moving from symmetric to slightly asymmetric energies in each of the two linacs.

For a symmetric linac configuration change, the beam energy change needed is ~ 93 MeV. This is a small enough fractional change in the total beam energy that the MOLLER apparatus can be designed to accommodate both energies for production running with no other changes. Of course, if an asymmetric linac configuration can be found that will maintain the total energy to be the same while accomplishing a polarization sign flip, that would be desirable. However, we do not believe this is a necessary constraint, especially if it complicates other aspects of beam quality.

Over the duration of all the production running, a total of 10 energy flips would be desirable, with at least one such flip during run I, 3 to 4 flips in run II and 6 to 8 flips in run III, or effectively a configuration change every 6 to 10 weeks during production running. The exact frequency and the nature of the configuration change would be chosen after detailed consultation with the Accelerator Division. Since the requested frequency for the configuration change is similar to that required for transverse running, it might well be optimal to schedule the required 100% transverse running in the period in which an energy configuration change is being made.

Appendix A

Liquid Hydrogen Target Update

The design of the target for this experiment, as described in the proposal, is predicated on several novel ideas which were to be tested for the first time with the Qweak target. The Qweak target, we argued in the proposal, is really the prototype for the Moller target. Although the Qweak target is still being commissioned and many of the key results are only just now coming to light, it is appropriate in this update to review what has been learned so far in order to see whether those Qweak ideas and design aspects crucial to the Moller LH2 target hold any water.

The most crucial aspect of the Moller target design which needs to be validated is the novel use of computational fluid dynamics (CFD) as a design tool. Computational fluid dynamics was used in almost all aspects of the design of the Qweak target. It was used to tailor the cell design in order to optimize the flow, temperature and density profiles across the beam axis in the hydrogen volume as well as at the cell windows. These simulations were used to fix the mass flow required of the target, one of the most crucial design parameters. The pressure head represented by the complicated cell shape was derived by CFD. Analytic calculations for the Qweak target's heater and some aspects of the heat exchanger were checked with CFD simulations. CFD simulations fixed the raster size required for the target and helped us design strategies for various off-normal events. In many respects the novel design which emerged was considered a bit of a gamble, given that CFD was not a proven tool for target design.

The 35 cm long, high power Qweak target has met its ambitious design goals, at least to the extent we have been able to measure them until now. The target has been successfully operated with 3 kW of cooling power, many times greater than any target previously built. It has been run routinely now with 150 μA of 1.165 GeV electrons. The target boiling contribution to the asymmetry widths in the experiment is too small to measure until now, although an upper limit of 100 ppm has been derived for the boiling contribution with indications it may be considerably smaller than this still. The bulk density changes have also been bounded to less than 0.2% at 150 μA . This should be compared to the performance of the standard pivot

15 cm machined cells, for which the density variation at 100 μA has been measured to be 20%, a factor of 500 worse. Although the design raster size for the Qweak target was 4x4 mm², the target's performance is so good that it is operated routinely at 150 μA with a raster size of only 3x3 mm².

The fact that the Qweak target has achieved all of its design goals validates the use of CFD as a design tool. We note that the matrix of 24 solid targets that are also part of the Qweak experiment were also designed with CFD. The relationship between temperatures at the center of each target to thermometry scattered around the solid target frame was studied with CFD. Knowing how high these thermometers can safely go, by virtue of the CFD calculations, has made it possible to put more beam current on our solid targets than has ever been done before at JLab.

It also shows that the heat exchanger design process used for Qweak was correct. Note that the Qweak heat exchanger is a completely novel design which combines a 4 K and a 15 K heat exchanger using overlapping heat exchanger coils in the same shell.

It also shows that the high power heater design and fabrication process was correct. The 3 kW heater performance is unmatched. When beam trips occur, or beam is restored to full current, the typical temperature excursions in the target loop thermometers are less than 0.1 K.

The pressure head predicted for the Qweak target at the design mass flow of 1.1 kg/s was 1.2 psi. The head measured with the Qweak target at this massflow is 1.1 psi, in amazingly good agreement with the prediction considering how very difficult it is to calculate this ahead of time. Note that head and massflow are the two most crucial design parameters for most of the target's components.

The fact that the required massflow and pressure head were achieved for the Qweak target also validates the pump design. Problems have been encountered with the Qweak pump bearings, which have led to some down time. However the basic deliverables of the pump (head and massflow) have been achieved at the required values.

Qweak initiated the use of faster helicity reversal as a tool to mitigate the effects of target noise on the experiment. Fast Fourier transforms acquired under a wide variety of conditions during the Qweak experiment's commissioning phase show that this is an important and effective tool for reaching the goals of the experiment, and its effectiveness for the Moller experiment is now also validated.

Qweak also pioneered the use of a recovery heat exchanger at the ESR in order to boost the effectiveness of the ESR by making use of the enthalpy of the returning 4 K coolant. The ESR recovery heat exchanger (designed by Rao Ganni) has proven to be enormously successful. It has boosted the 15K cooling power the ESR can deliver by about 50%.

Another novel design feature now validated by Qweak is the re-configuration of the existing transfer line infrastructure in order to simultaneously supply both 4 K coolant and 15 K coolant to the target, and in particular, to return both coolant

sources on separate lines back to the ESR. This required using the LN2 supply shield as a 20 K helium return. A small superconducting polarimeter magnet in the Qweak experiment is also fed and successfully operated with this highly unusual configuration.

A director's review of JLab cryogenic capacity has been held. The final report is available at

http://www.jlab.org/div_dept/dir_off/ccr/.

The Moller experiment's 5 kW cooling power requirement figures prominently in the report. The report states that the planned ESR #2 by itself has the 5 kW capacity required for the Moller experiment. The ESR #2 building is currently under construction, and the refrigerator has been designed (but not yet funded). However, the first of the director's review committee's recommendations is that funding be secured for ESR #2 on a timeline that makes it available for the Moller experiment, as early as 2015. Finally, the report also recommends (on page 5) that the Hall A 4K transfer lines be re-evaluated and upgraded for the 12 GeV era in part because they have unusually high heat loads associated with them, and in part to better meet the demands of the 12 GeV era (such as the Moller experiment).

To summarize: the Qweak target employed a large number of novel and highly unusual ideas to meet its goals. We now know that every single one of these new ideas has worked. This greatly reduces the risk associated with the extensions needed for the Moller target. The cooling power needed for the experiment has been carefully considered by the lab and solutions are already under way that will insure the experiment's requirements can be met.

Appendix B

Spectrometer Design

B.1 Spectrometer

A great deal of work has been devoted to the design of the spectrometer since the proposal. The spectrometer consists of two toroidal magnets, each with 7 coils equally spaced around the azimuth, which focus the Møller electrons radially and azimuthally at the detector plane. As described in the original proposal, the spectrometer makes use of the fact that we are considering identical-particle scattering. Thus we obtain 100% azimuthal acceptance by accepting backward scattered Møllers, which have lab scattering angles of 5.5-9.5 mrad, and forward-scattered Møllers from 9.5-17 mrad in a particular phi bite (open sector), leaving the diametrically opposed phi bite available for placement of the coils (closed sector). The upstream magnet, despite the small radial size compared to its length along the beamline, is a conventional toroidal magnet. The downstream magnet is a novel design, the geometry of which helps to focus Møller electrons with a large range of scattered angles and energies (5.5-17 mrad and 2.5-9.5 GeV).

Most of the work that has been done was for the hybrid magnet, although the upstream torus has also been updated with a realistic conductor layout. The hybrid magnet has undergone several iterations using a commercially available software package available from Vector Fields, called TOSCA, to design the coils and produce fields maps, which are then imported into a GEANT4 simulation which includes radiative losses. The first step was verification of the field used in the proposal, both through direct comparison of the fields and in the result of GEANT simulations. The design of both magnets now includes suggestions made by engineers during the first engineering review, held on August 31, 2010, which will be discussed in Section B.4. The current design is shown in Figure B.1. There is now a design which includes an actual conductor layout with reasonable electromagnetic and water-cooling properties, which is being optimized for desirable optics properties while staying within the engineering constraints.

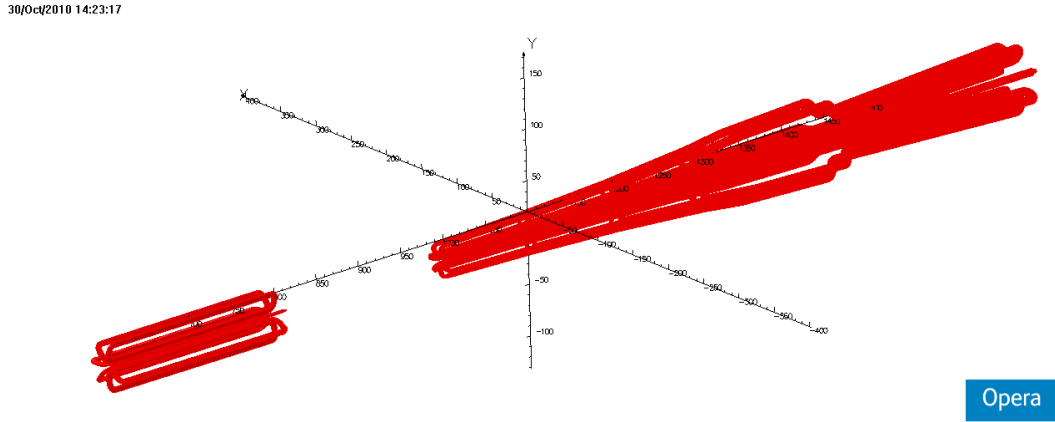


Figure B.1: Current design of the spectrometer which was developed using TOSCA.

B.2 Verifying the Proposal Field

The field map that was used in the proposal was generated with a “home-built” code, written expressly for the optimization of the hybrid spectrometer. It is a great success that the map was reproduced independently using TOSCA, and the values of the fields in the two maps can be directly compared. There are 3 components to the field (B_x , B_y and B_z) at each individual point in space, so it is difficult to show the agreement here with limited space. The individual cartesian components of the field, in bins of radius vs. azimuthal angle, ϕ , for a z location 12 m downstream of the target is shown in Figure B.2. The field gets large near the physical locations of the coils, and in the original proposal map there are some discontinuities which occur for the calculation of the field within the location of the coils. The TOSCA calculation appears more smooth.

In this sector B_x is primarily the azimuthally focusing component, and B_y the radially focusing component. The component in the z direction is very small. It should be noted that, because this is not a perfect toroid, the field components vary as a function of ϕ for a given radius. This affects our ability to radially focus Møllers that are scattered at large azimuthal angles. In addition, near the outer radius the field is azimuthally de-focusing. Because most of the tracks pass through the upstream torus between the low radius parts of the coils, the upstream torus focuses them azimuthally, and this effect is exploited in the design of the spectrometer.

Figure B.3 shows the excellent agreement between even the relatively small azimuthally (de-)focusing component of the field (left) between the two maps at a radial location of 15 cm, in 5° bites in ϕ vs. z . The right shows the agreement for the radially focusing component. The red points are from the original proposal map, and the black points are from the TOSCA map. There is a bit more spread in the field values from the proposal map at ϕ values close to the coils (which are centered

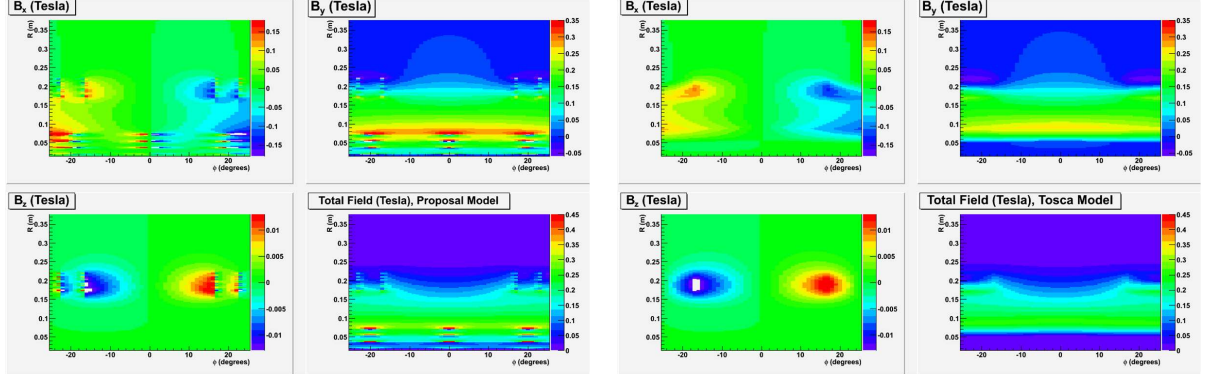


Figure B.2: Plots of the cartesian field components (B_x , B_y and B_z as well as the total field) in one sector for the original proposal magnetic field map (left) and TOSCA version of the proposal map (right). The field values are plotted in bins of R vs. ϕ for a z location of 12 m from the center of the target.

at $\pm 25^\circ$), consistent with what is shown in Figure B.2.

Reproducing the proposal field in TOSCA had a dual purpose. One was to check that the assumptions made with the field map produced for the proposal were valid. The other was to gain experience with using TOSCA. There were slight differences in the fields due to actual differences in the coil geometry as defined in the code used to calculate the proposal model compared to TOSCA (see Figure B.4). The proposal model used line currents, and the coils in TOSCA are defined as trapezoidal blocks. The overall agreement was quite good, with the largest differences less than 10% where the geometry differed significantly. Further effort to make the models agree more closely would likely be wasted, mostly due to the difficulty of defining the coils in TOSCA compared to the way they were done in the proposal model.

In addition to direct comparison of the fields, maps were produced in TOSCA which could then be read into the GEANT4 simulation. While tracking of scattered particles with an energy dependence on scattering angle is relatively easy in TOSCA, the GEANT4 simulations are necessary to incorporate energy loss in the target and other radiative effects. Some results of the simulation are shown in Figure B.5 for tracks at the focal plane, which is located 28.5 m downstream of the center of the target. Again, the agreement between the simulations using the two fields was quite good, and further work to reproduce the proposal field was abandoned in order to move forward with the design of more realistic coils.

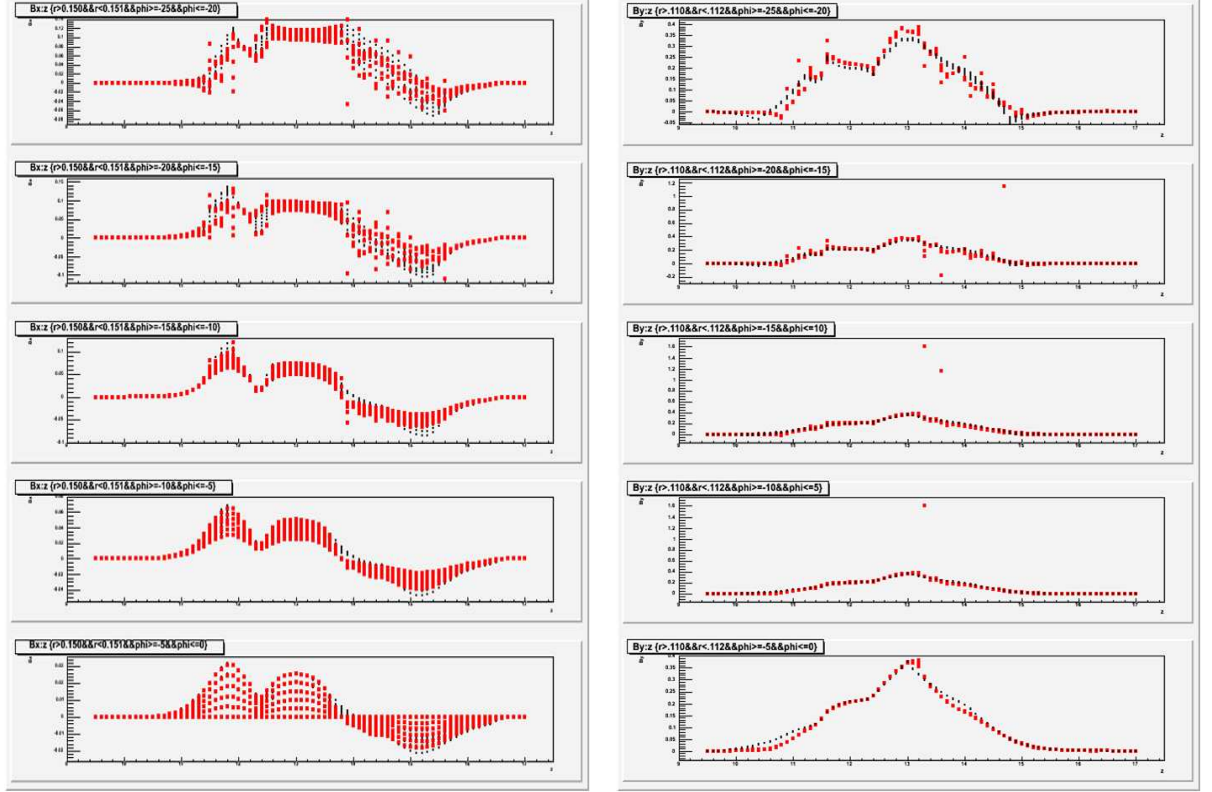


Figure B.3: The azimuthally focusing component (left) and radially focusing component (right) of the TOSCA (black) and original proposal (red) field maps vs. z at radius of 15 cm for different 5° portions of the azimuth from -25° to -20° (top), down to -5° to 0° (bottom).

B.3 Towards a More Realistic Magnet Design

In order to prepare for the first engineering review, held on August 31, 2010, a more realistic magnet design was developed using TOSCA. For the original proposal, the field map was produced using a Biot-Savart calculation of line currents. The design that was presented in the proposal consisted of four segments with different amounts of current in each segment. The amount of current increases going downstream. This is done in order to optimize the amount of field seen by the Møllers compared to the elastic ep scattered electrons. Because the electrons produced in the elastic ep process have more energy, there is some radial separation within the length of the magnet, and it can be designed so that in the segment at the end of the magnet (the one with the largest current) the Møller electrons are outside the inner radius of the coils, while the ep scattered electrons are below it and see much less field.

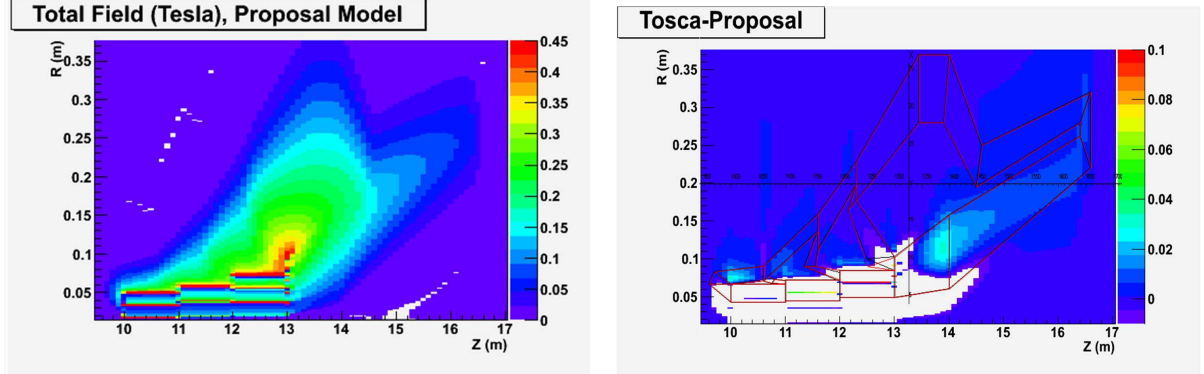


Figure B.4: The total average field in a sector for the proposal map is shown on the left. On the right is shown the difference (in Tesla) between the average fields in a sector for the TOSCA and original versions of the proposal, with the coil geometry superimposed. Non-zero differences arise due to slight differences in the actual geometrical definitions of the coils. The white region is where there are non-physical values of the field within the actual coil definition.

Any design of the magnet will have to utilize this feature.

The calculation of the field map optimized the current in each segment without taking into account the size of the conductor, which means that the currents in each segment and the difference in the currents from segment to segment were not necessarily integer multiples of any particular amount. TOSCA was used to define individual wire turns with actual dimension in a coil layout that included actual conductors with space for insulation. The first step in this process involved trying to fit wires of various sizes into the radial and azimuthal extent of the coils given by the proposal model and the relative currents between the different segments of the hybrid toroid. This resulted in a large number of out-of-plane bends to fit into a large ϕ extent (nearly the full azimuth) at low radius but transition to smaller than half of the azimuth at large radius.

Additional constraints that were taken into account in the design of the actual conductor layout include the minimum bend radius of the wires (5x the wire outer diameter (OD)) and the current density. The transition from the third segment into the most downstream segment, where the current is greatest and hence the number of wires is greatest, proved to be the limiting factor. The coils no longer fill the full azimuth at low radius along the whole length of the magnet, although they mostly fill it at this transition. The choice of conductor size did not seem to impact the current density, so an optimum conductor size was chosen based on whether the relative currents between segments was similar to the proposal.

This version of the hybrid torus (called version 1.0) produced physics results

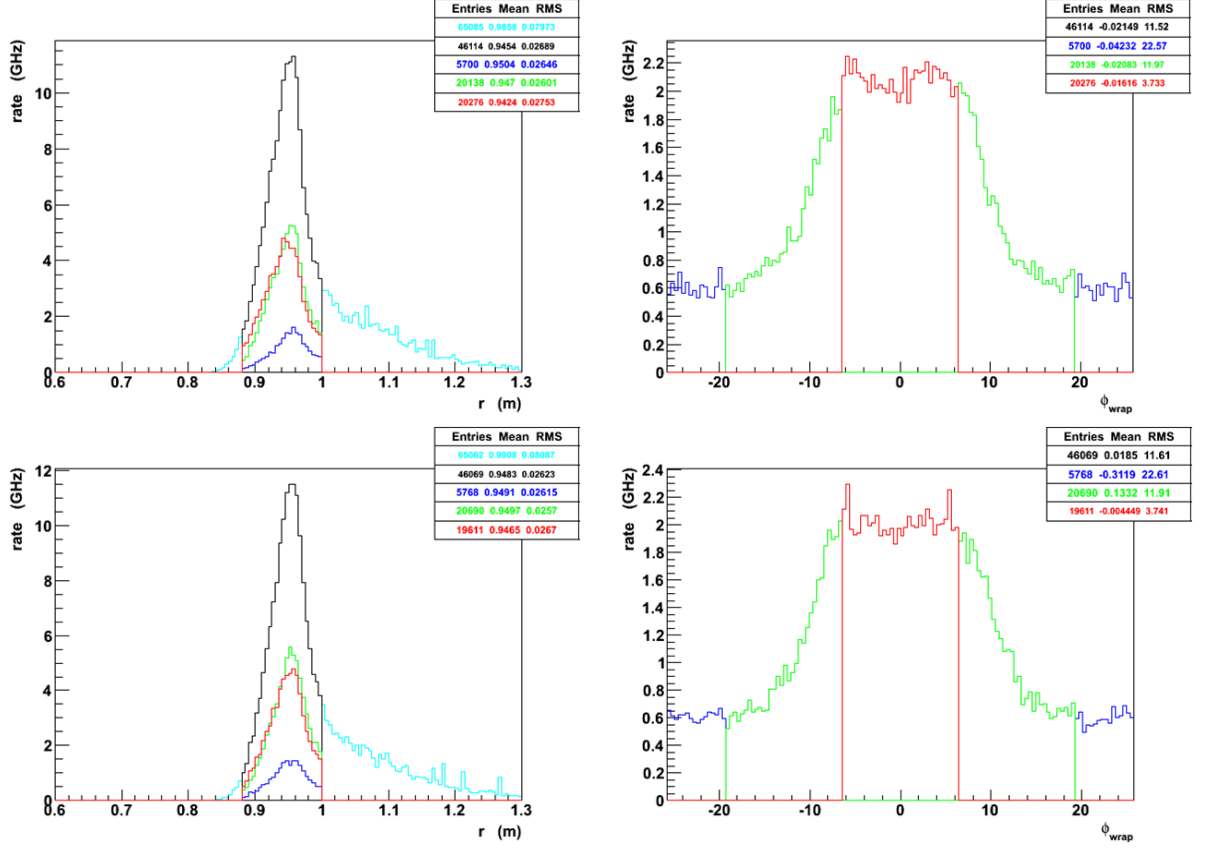


Figure B.5: The top two plots are from the GEANT4 results using the original proposal map, the bottom two plots used the TOSCA version of the proposal map. The plots on the left are for the radial distribution of events at the detector plane; the plots on the right show the ϕ location at the detector plane. The colors indicate whether the tracks are in the center of the open sector, the center of the closed sector, or straddle the open and closed sectors when they hit the detector plane (red, blue and green, respectively).

that were qualitatively similar to the proposal model. The radial focus occurs at a larger radius, which may be preferable for reducing photon backgrounds using shielding. Unfortunately it is also a bit wider, which adversely affects the background fraction from elastic ep electrons, and from other sources of background as well. According to GEANT4 simulations the Møller rate without optimizing the collimators is higher (see Table B.3), but so is the background from the elastic eps. Further work would be needed to optimize this version, including revisiting the collimation. However, this version was put aside in favor of one which takes into account the suggestions made by engineers during the first magnet review. Opti-

Table B.1: The number of wires and currents in the different segments based on the choice of conductor size. The segments under consideration are those that are defined as the inner radial parts of the coils in the different segments, with X being the most upstream, smallest current, and then Y, Z, and into A, which is the segment which contains the maximum current. The current density in each case is at least 1550 A/cm^2 . The conductor with an OD of 0.4620 cm is the one presented at the magnet review. The last row is the one used based on the comments from engineers.

OD (cm)	A_{cond} (cm^2)	Total # Wires				Current (A)				\vec{J} (A/cm^2)
		X	Y	Z	A	X	Y	Z	A	
Proposal	—	—	—	—	—	7748	10627	16859	29160	1100
0.4115	0.1248	40	54	86	146	7989	10785	17176	29160	1600
0.4620	0.1568	32	44	70	120	7776	10692	17010	29160	1550
0.5189	0.1978	26	36	56	94	8066	11168	17372	29160	1568
0.5827	0.2476	20	28	40	76	7680	10752	15360	29184	1551

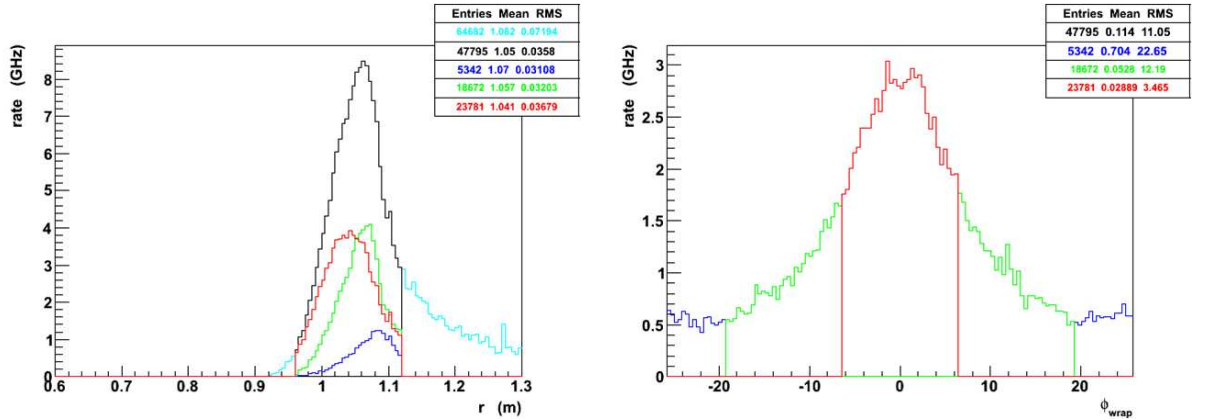


Figure B.6: Plots from GEANT4 simulations which used the field map produced using the actual conductor layout designed in TOSCA. The plot on the left is for the radial distribution of events at the detector plane; the plot on the right shows the ϕ location at the detector plane. The colors indicate whether the tracks are in the center of the open sector, the center of the closed sector, or straddle the open and closed sectors when they hit the detector plane (red, blue and green, respectively).

Table B.2: Comparison of various quantities for the two versions of the actual conductor layout. Concept 1 is what was presented at the magnet engineering review. Concept 2 takes into account suggestions made by the engineers at that meeting. *Note that the length is estimated for the longest turn only.

	Concept 1	Concept 2
weight _{coil} (lbs)	556	555
R _{coil} (Ohms)	1.98	0.741
V _{coil} (V)	480	285
I _{wire} (A)	243	384
P _{magnet} (kW)	820	765
\vec{J} (A/cm ²)	1600	1551
L _{turn} (m)	15*	15*
# turns	120	76

mization that as occurred as of the writing of this update for that version will be discussed in Section B.5.

B.4 Engineering Review

The first magnet review was very productive. The design as described in Section B.3 was presented to a panel of 6 engineers: George Clark (TRIUMF), Ernie Ihloff (MIT-Bates), Vladimir Kashikhin (Fermilab), Jim Kelsey (MIT-Bates), Dieter Walz (SLAC), and Robin Wines (JLab). In general the comments were positive and/or constructive, with nothing that would prevent the operation of the magnet, although there was no presentation of magnetic forces or a detailed study of positioning tolerances, which we hope will be available for the next magnet review, which is yet to be scheduled. The concerns that were raised involved water-cooling issues, including the size of the conductor/water-cooling aperture and the many bends in the design. Other issues included concerns about placing the coils around the “petal” vacuum volume and the lack of a support design. Requests for the next review, besides addressing these issues, included a better description of the geometry of the field (made difficult in part because of the hybrid nature of the magnet).

There was not much concern about the size of the current density in the coils, but rather more concern over the size of the water-cooling aperture. It was noted

that the water could simply be flowed faster and/or be chilled, but that the design with this small of a conductor would likely be too complicated to be realistic because there would be too many connections. It was a general consensus that a water-cooling hole of at least 0.125 inches would eliminate concerns about back-flows, eddies and build-up of oxides that could cause a plug and affect the long-term operation of the magnet. They agreed that the minimum bend radius should be 5x the conductor OD. It was suggested that a larger conductor may also reduce the “waves” down the length of the magnet that will be introduced during manufacture of the coils. We were cautioned against using two different conductor sizes, which would necessitate using different power supplies. So, the new design uses a larger conductor and has as few out-of-plane bends as possible, which results in about 38 water connections per coil (for supply and return).

A new design for the coils has been developed which takes into account these suggestions (see the last row in Table B.1). Because there are fewer conductors and they have a larger cross-section, the power in the magnet is slightly lower and the voltage per coil is almost half of what it was in the first actual conductor layout (see Table B.2). Optimization for physics optics results should not change the design of the magnet to the point where the support concept could not be easily adapted, so this updated version has been sent to JLab engineers for design of structural supports and water-cooling system. It was suggested during the meeting that the coils should be mounted inside the vacuum volume due both to space constraints and the complicated nature of the vacuum volume as proposed making it hard to be ASME compliant. The engineers suggested that it should be straightforward to stiffen the coils with G10 or carbon but cautioned that whatever epoxy or insulator we used would have to be radiation hard.

Work since the meeting has included estimates of the magnetic forces on the coils and determining keep-out zones which will help minimize the position sensitivities (which were taken into account in the updated design). The preliminary results from the study of the magnetic forces using TOSCA is that the centering force on the coils is about 3000 lbs., or 5500 lbs. on the inner part of the coil (inward) and 2600 lbs. on the outer part of the coil (outward). This can be compared to QTOR, the Qweak magnet, which has a centering force of 28,000 lbs. per coil (which was also verified within a factor of 2 using TOSCA). The effect of asymmetrically placed coils and coil motion upon being powered up need to be studied and taken into account in the design of the supports.

Some other suggestions that were made include the use of steel which would increase the field and decrease the forces, eliminating the lowest current, most upstream part of the magnet, checking the tolerances because of the large variation in the radially focusing field and the possibility of introducing iron poles in order to reduce the size of the coil cross-section. In general we want to avoid any magnetic material because of backgrounds, so the steel and the iron poles will be kept in reserve for now. The upstream part of the magnet helps to separate the Møllers and

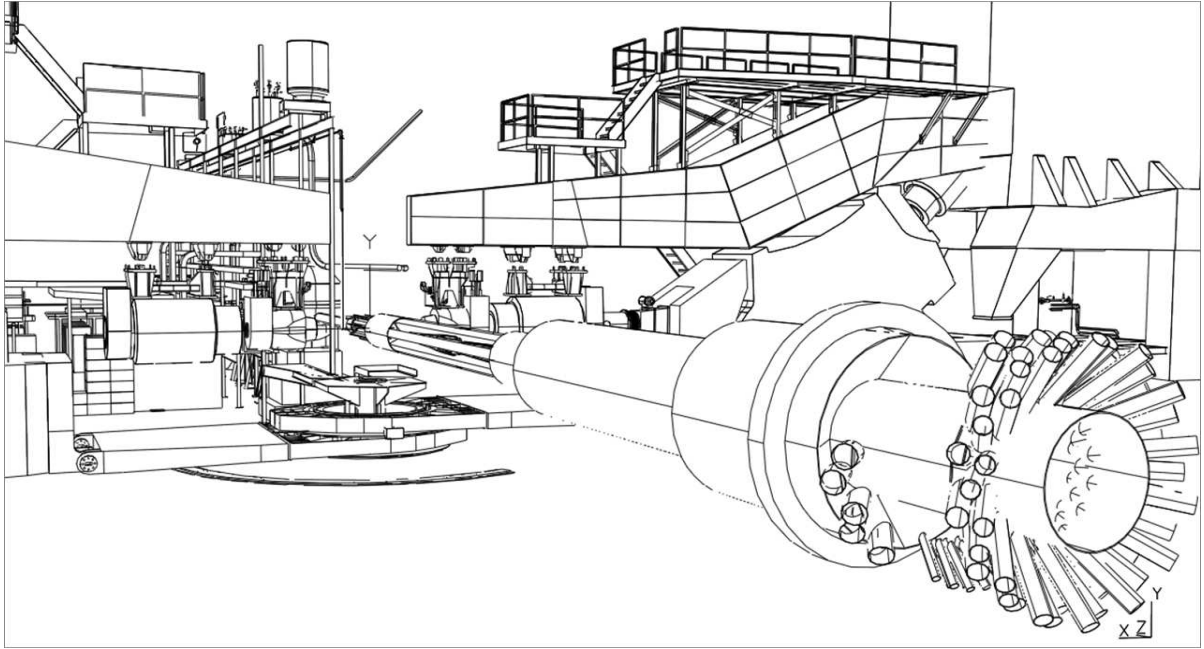


Figure B.7: Current design placed in Hall using TOSCA step file.

the electrons that underwent elastic ep scattering, so we need that in order to make the rest of the magnet more effective. A detailed sensitivity study will be done for a design that is more optimized from an optics point of view.

B.5 Optimizing for Physics Considerations

The design that was achieved for the proposal field map was very robust, and the qualitative performance was not too adversely sensitive to the initial changes in the coil geometry going from the line current model to an actual conductor layout. The first actual conductor layout was chosen specifically to keep the relative currents between segments as close to the proposal model as possible. As a result of the changes adopted to meet the engineers' recommendations, however, the optical properties of the magnets changed somewhat more significantly (see Figure B.10). It should be possible to optimize the magnet by making judicious changes that will maintain the necessary engineering aspects of the current design.

The optimization is faster than with the home built code. TOSCA is used to make the changes to the geometry, and tracks are generated which can be used to gauge the effect on unradiated Møller and elastic ep scattered electrons which have the correct energy-angle dependence (see Figure B.8). This is a relatively fast turn-around, making use of the "coils only" calculation due to the fact that so far, all of our materials are linear. If this were not the case, it would be necessary to use

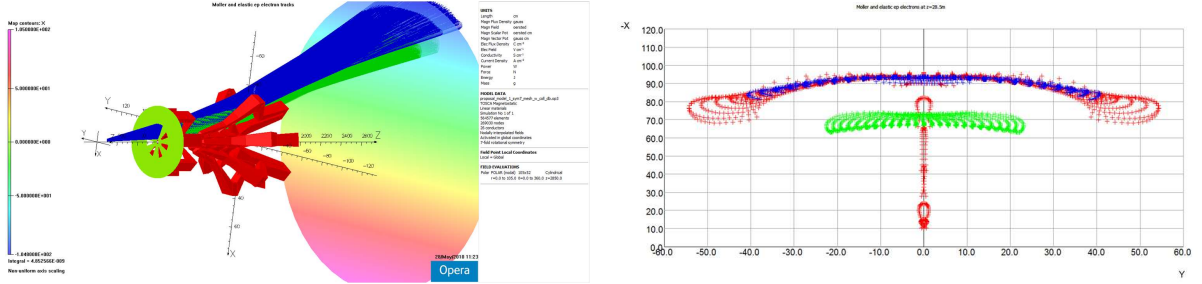


Figure B.8: The figure on the left shows Møller (blue) and elastic ep (green) tracks generated in TOSCA, with a collimator in place. The plot on the right shows the same tracks at the intersection of a plane at the detector location (Møller tracks with no collimation are shown in red).

the finite element analysis capabilities of TOSCA. A “blocky model” of the actual conductor layout is used to reduce the calculation time (see Figure B.9). Tracks for 3 geometries are generated simultaneously on a machine purchased by UMass for this purpose (the limit of 3 is due to the number of available licenses being 4, and leaving one open for use by another JLab user, not a limit of the machine itself). The tracks can be examined in 3 dimensions within the framework of TOSCA, which allows for the identification of interferences with the coils. They also can be plotted at the intersection of a plane which shows the X:Y distribution at the detector plane so that the separation between the ep and Møller peak can be taken into consideration.

The major difference between the proposal model and the model that takes into account the recommendations of the engineers is that the radial focus is a bit wider, which makes the background fraction higher (see Figure B.10). In order to explore the possibility of improving the radial focus, two changes to the geometry of the magnet were explored. One is to change the angle of the tail of the magnet to minimize the field seen by the elastic ep scattered electrons, while ensuring that the Møllers still see as much field as possible. In order to improve this, the field in the upstream magnet was increased (the current density with the increased field is 1352 A/cm^2). The other change is to reduce the radius of the outer part of the coil in order to minimize the field seen by the high angle scatters, thus focusing them better at the detector plane. This change has the adverse effect of reducing the separation between the ends of the Møller distribution and the elastic ep distribution.

The focus is somewhat better for Møllers with low scattering angles, which increased the overall Møller rate even in the first actual conductor layout compared to the proposal (see Table B.3). It should also be possible to trim the acceptance a bit, maintain a relatively high Møller rate but reduce the size of the radial distribution at the focal plane and thereby reduce the background fraction. The accepted angular range is also bigger than it needs to be from the point of few of full az-

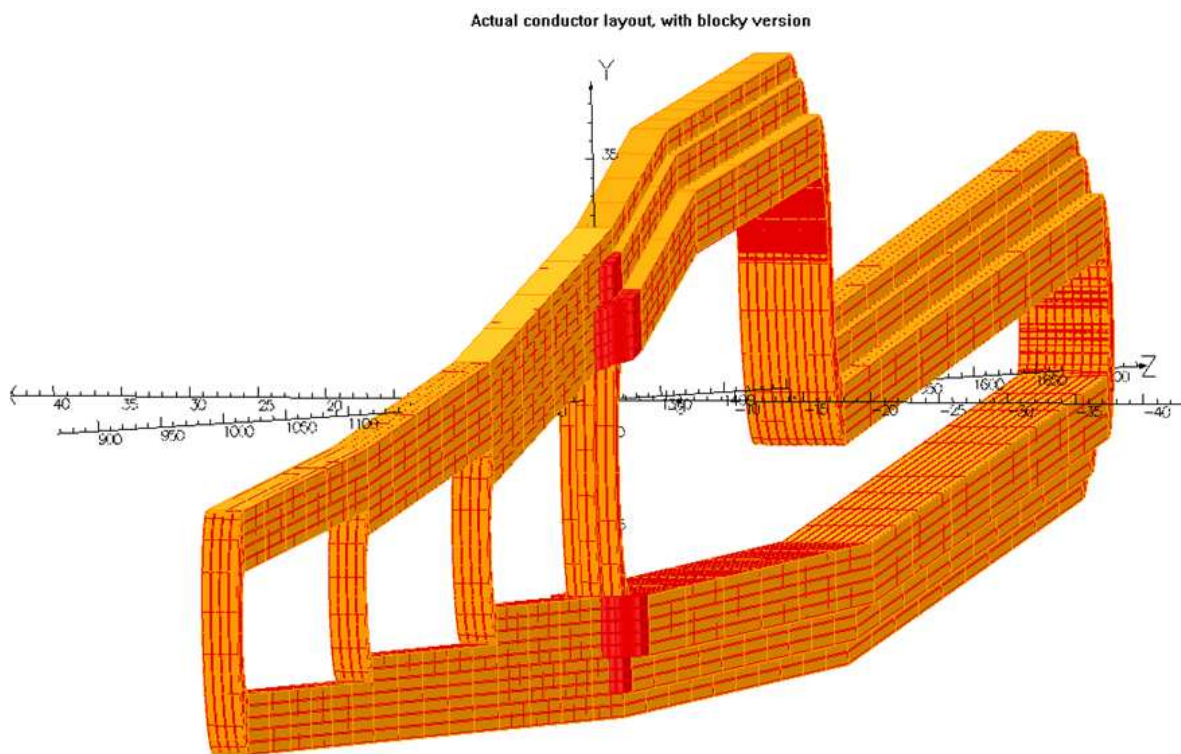


Figure B.9: The actual conductor layout of the model which has been updated to take into account the recommendations from the engineers as a result of the magnet review. The actual wires are shown in red, and the blocky model which is used in the optimization is shown in orange.

imuthal acceptance. That is, we only really want high angle scatters that have a corresponding low angle “partner” accepted, as described above and in the original proposal in more detail.

As the optimization for physics considerations nears completion, it will be necessary to revisit the collimation, both from the point of view of reducing the angular acceptance based on the studies described above, but also to reduce the photon background. The collimation that is currently being used is the same as what was used in the original proposal and has not yet been optimized for the present magnet design. Once the optics have been optimized in TOSCA, the collimation will be optimized for that version, and if necessary the magnet design could be tweaked as well. The radial focus is at a larger radius, which should help from the point of view of shielding the photon background, and reducing the size of the radial focus should help as well.

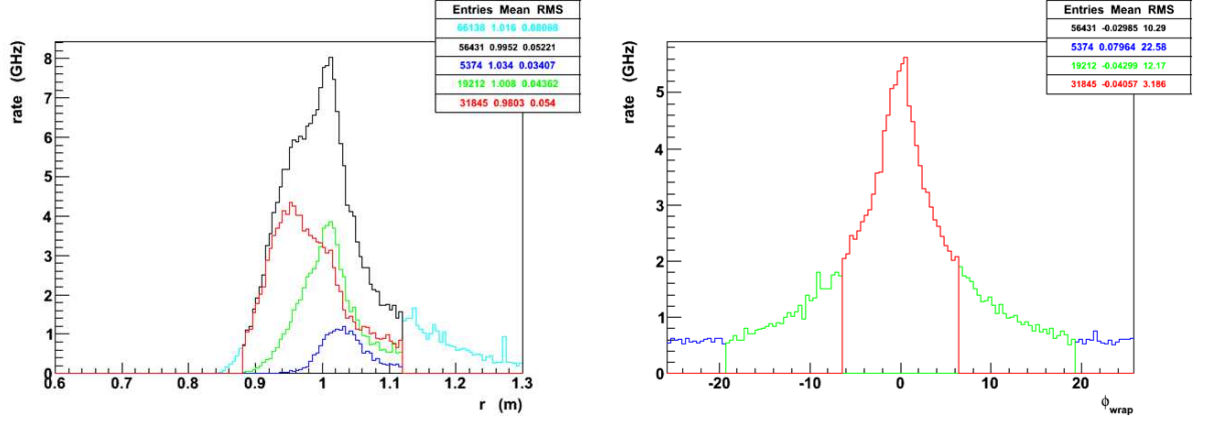


Figure B.10: Plots from GEANT4 simulations which used the field map for the design updated based on the feedback from the engineering review. The plot on the left is for the radial distribution of events at the detector plane; the plot on the right shows the ϕ location at the detector plane. The colors indicate whether the tracks are in the center of the open sector, the center of the closed sector, or straddle the open and closed sectors when they hit the detector plane (red, blue and green, respectively).

Table B.3: Estimated rates for various simulated processes in the radial bite chosen for the detectors, according to the GEANT4 simulation for different versions of the field maps.

Field Map	Møller (GHz)	Elastic ep (GHz)	Inelastic ep (GHz)	Bkgd. Fraction (%)
Proposal	151	13.7	0.5	9
Actual (v1.0)	184	20.2	0.7	10
Actual (v2.6)	192	28	0.9	13
Actual (v2.11)	194	27	0.9	13

Appendix C

Backgrounds Update

C.1 Correction from Inelastic e-p Scattering

The strategy to correct the raw Møller asymmetry for the asymmetry in the inelastic background is to make a direct measurement of inelastic e-p asymmetry in auxiliary detectors. Accordingly, we have optimized the radial segmentation of the integrating quartz detectors as shown in Fig. C.1. Bin 5 is the Møller peak, while bins 3 and 4 have significant contributions from inelastic scattering; their asymmetries will be completely dominated by the contribution from the vector coupling to inelastic states.

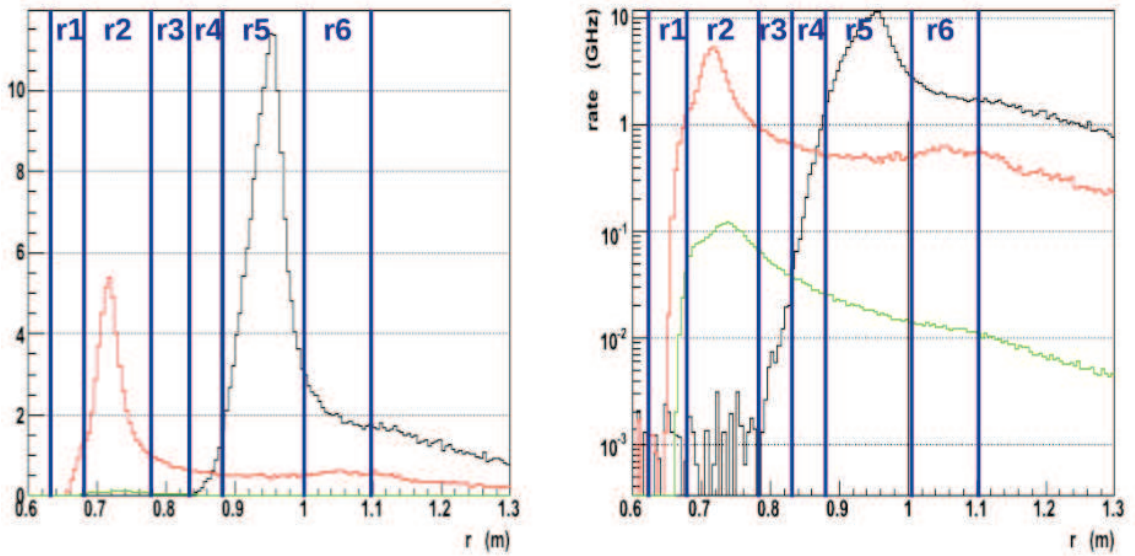


Figure C.1: Proposed radial segmentation of the scattered electron flux, shown both in linear and log scale. The black, red and green curves are for electrons from Møller, elastic e-p and inelastic e-p scattering.

We next look at the W^2 distribution of the inelastic events in the various radial bins. We find that the azimuthal binning into the red, green and blue sectors¹ provides important variation in the W^2 distribution that facilitates extraction of the inelastic asymmetry for different ranges of W^2 . This is demonstrated in Figs. C.2 and C.3, which are the W^2 distributions for the three different azimuthal sectors in bins 5 and 4 respectively.

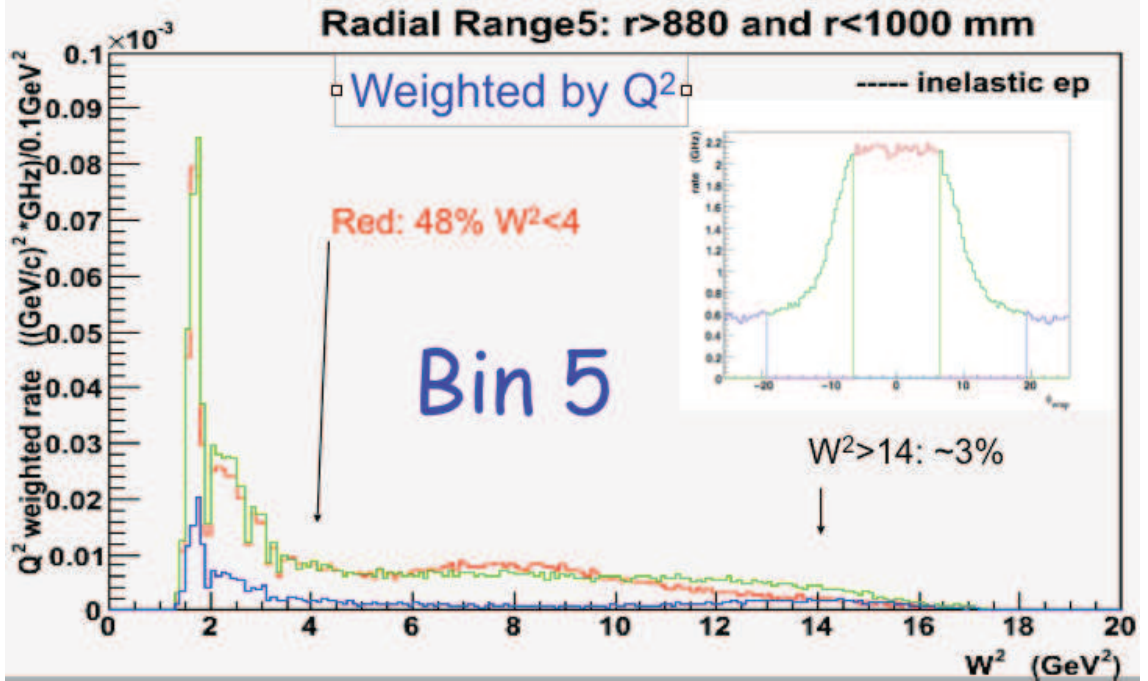


Figure C.2: W^2 distribution for red, green and blue sectors (see inset figure and footnote below) in Møller peak radial segment (Bin 5).

We then empirically found combinations of azimuthal sectors in Bins 3 and 4 that mimic the shape of the W^2 distributions for inelastic e-p events in Bin 5. If they match well, it would imply that measured asymmetries in the same bins can be used, with the same linear combinations, to correct for the inelastic background in the Møller peak (Bin 5). Fig. C.4 shows an example of how well this works for one such combination. We conclude that a careful analysis should allow us to reliably make corrections for the inelastic background and the systematic error from the correction should be small compared to the statistical error.

¹The azimuthal segmentation of the detectors is described in Sec. B6 of the original proposal document.

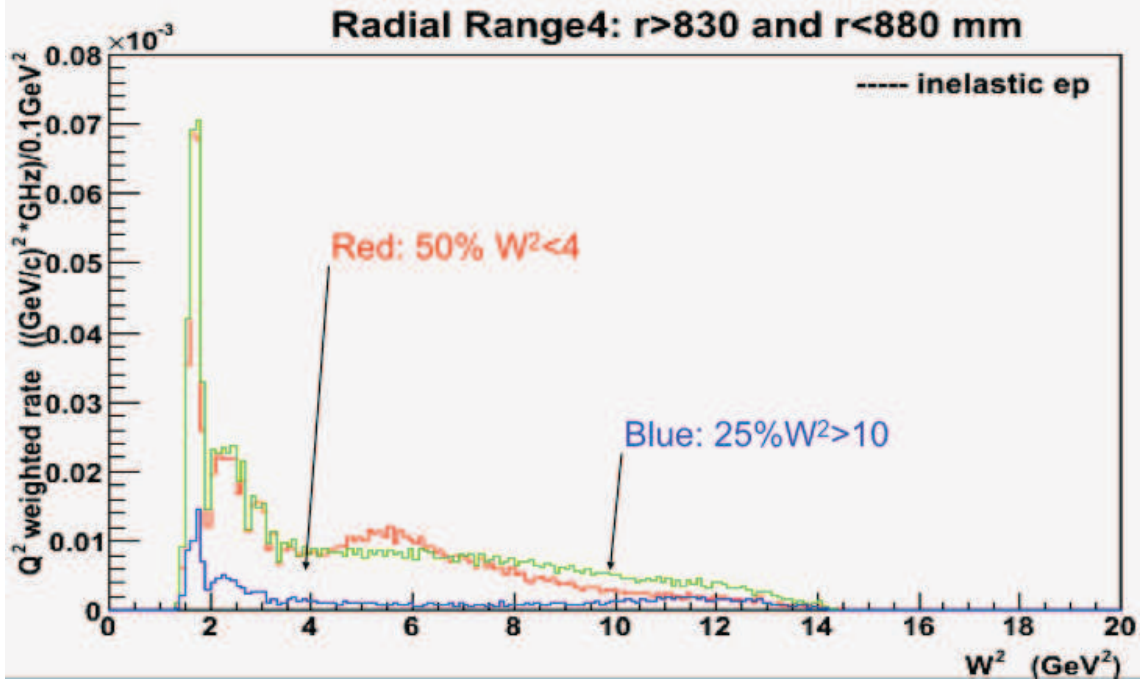


Figure C.3: W^2 distribution for red, green and blue sectors in Bin 4.

C.2 Pions from Weak Decays

We have launched a detailed study of exclusive hadron electro- and photo-production, using E158 pion background studies as a starting point. Using very conservative assumptions, we used published data from 11 GeV electro-production at Cornell [5], and an analysis [6] by the COMPASS collaboration on polarization transfer in hyperon production in polarized muon and neutrino beams, to estimate that the fraction of the pion flux at E158 from weak decays is $\sim 6 \times 10^{-4}$ and that the polarization transfer is of order 5%, leading to a pion asymmetry of 3×10^{-5} . Since the measured pion asymmetry at E158 was 6×10^{-7} , this is a factor of 50 overestimate.

We now use the result of a detailed analysis of SLAC data [7] on exclusive production of hadrons to rescale the flux for a 11 GeV beam and deduce that the fraction of pions from weak decays in MOLLER would be 3×10^{-5} . The total pion flux relative to the Møller electron flux should remain roughly the same (6×10^{-3} for thin quartz, factor of 5 less for the quartz/tungsten sandwich). If we assume the same 5% polarization transfer and the same factor of 50 additional suppression observed in E158, then the false asymmetry induced is 0.18 ppb for thin quartz, and correspondingly smaller for a “shower-max.” detector.

Our next task is to incorporate the detailed kinematic dependences as derived from previous analyses of world data into a Monte Carlo study to arrive at more

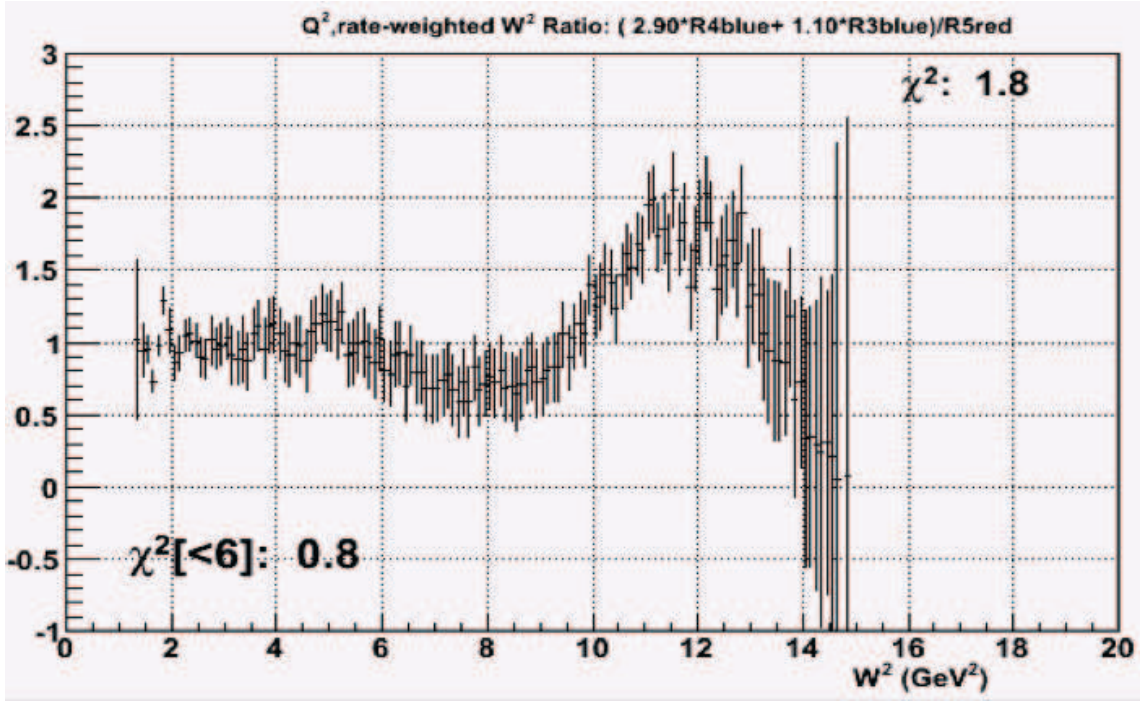


Figure C.4: Ratio the W^2 distribution of a specific linear combination of 2 inelastic bins to that of one of the primary Møller bin. It can be seen that they match very well for $W^2 < 6$ GeV².

accurate estimates for the E158 spectrometer configuration. This might shed some insight into the additional suppression over the naive estimate. We will then carry out a similar study for the MOLLER spectrometer configuration. In parallel, we will launch a study of how best to monitor and correct for such an asymmetry by making parasitic measurements of the rate of pion production and the parity-violating asymmetry that results, so that a reliable correction can be made even if it is as large as several ppb.

Appendix D

Tracking System

D.1 Tracking

As was mentioned in the original proposal, the MOLLER experiment will require a charged-particle tracking system, which will be used for diagnostic studies at very low beam currents. The motivation for such a system includes its use to help characterize background contributions, to characterize the spectrometer, and to determine the effective kinematics of the asymmetry measurement. Here we provide some detail on these motivations, and discuss our initial concepts for the tracking system design. Much of this discussion is informed by our experience from the HAPPEX experiments, E158, and most relevantly, recent experience with the Qweak tracking system.

D.1.1 Backgrounds and Spectrometer Optics

An important component to the systematic error on the asymmetry measurement will be the contributions from various background processes, including elastic electron-proton scattering (“elastic e-p’s”), inelastic e-p’s, neutrals (photons and neutrons), and pions and their decay muons (from real and virtual photoproduction in the target, and also deep inelastic scattering). The expected dominant dilution to the signal will be from the elastic e-p’s. The inelastic e-p’s will be much smaller in relative rate, however they will carry a larger and less-predictable asymmetry, and thus are a major concern as well. An important criterion for the spectrometer, detector and collimator design has been to ensure a “two-bounce” system in order to suppress neutral backgrounds, however at the high luminosity the experiment will run at, it is likely that there will still remain some neutral component to the integrated signal read out by the main detectors, which will dilute the measured asymmetry. Pions and decay muons can be produced from a variety of sources, and so their asymmetry will be hard to predict. Thus their asymmetry must be measured and their contributions to the yield must be determined, in order to correct for their

effect.

Much of the background identification and suppression provided by the spectrometer and main detectors has been described in detail in the proposal. A critical feature is the high degree of segmentation of the detectors in both radius and azimuth, which then provides asymmetry measurements in r, ϕ bins, which contain different mixes of signal and background processes. As an example, Fig. D.1 shows the simulated radial distribution of Møller electrons, elastic e-p's and inelastic e-p's, demonstrating the radial part of the kinematic separation. The shapes of the distributions are sensitive to not only the spectrometer optics, but also large radiative effects and multiple scattering in our thick (17% of a radiation length) hydrogen target. However, this figure is somewhat misleading: the radial segmentation of our main detectors is rather coarse on this scale. The same simulated data, binned as the detectors will be, is shown in Fig. D.2. Clearly, a meaningful comparison of the observed distributions of rates with the Monte Carlo prediction would be compromised by the coarse binning.

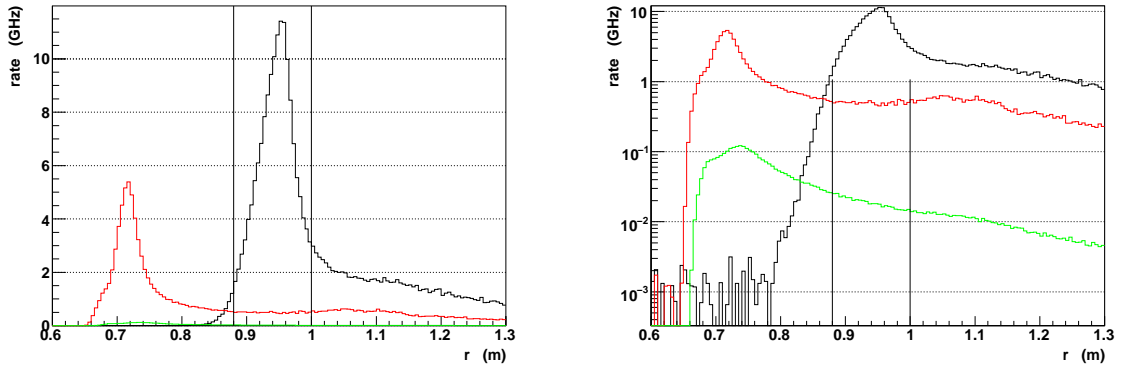


Figure D.1: *Expected rates vs. radial position for elastic e-p (red) electrons, inelastic e-p electrons (green) and Møller (black) electrons at the z location of the main detectors. Bins are 5 mm wide. The black vertical lines represent the edges of the main Møller detectors ring. Left: linear scale; Right: log scale.*

Similarly, the azimuthal distribution of tracks at the main detectors provides another tool for separating backgrounds. Figure D.3 shows the (r, ϕ) distribution of Møller and e-p electrons at the z location of the main detectors. As described in the proposal, the detectors will also be segmented azimuthally, with each sector of the spectrometer divided into four ϕ segments. This segmentation will provide some handle on verifying this distribution, but a detailed comparison with the simulated rates would require a finer spatial resolution than the detector segmentation will provide.

Thus, we propose a fast tracking system that will allow us to measure these rate

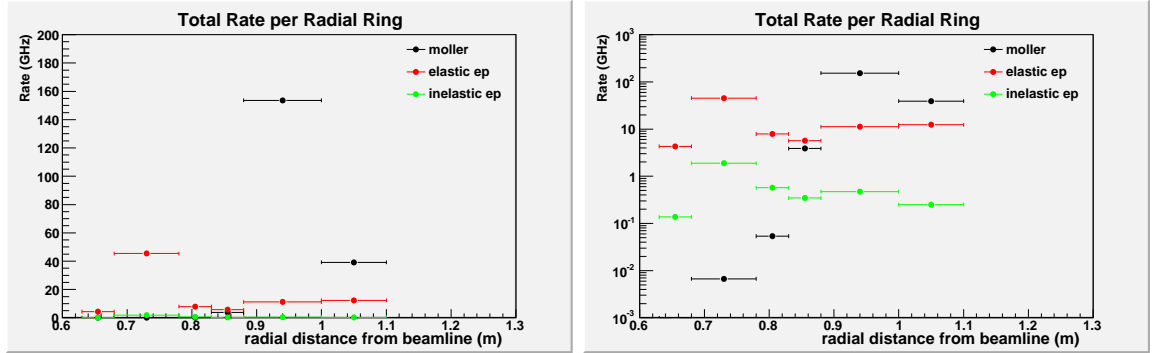


Figure D.2: *Same as Fig. D.1, except binned by the sizes of the various main detector rings. Left: linear scale; Right: log scale.*

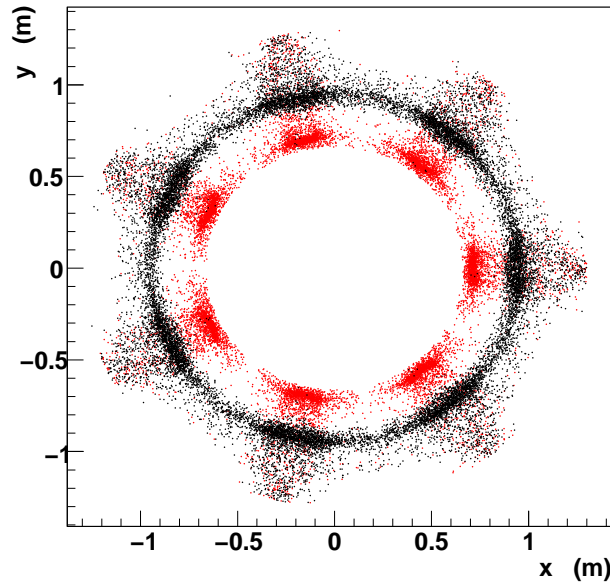


Figure D.3: *Expected distribution of events at the z location of the main detector from Møller electrons (black) and e - p electrons (red).*

distributions with fine position resolution (of order $250 \mu\text{m}$). The tracking system will be run with the beam current turned down to the scale of 100 pA , which will produce a total electron flux after the second toroid of $\approx 150 \text{ kHz}$ over the full azimuth, corresponding to a modest flux of $\leq 200 \text{ Hz/cm}^2$ at the main detectors. This should not tax the capabilities of conventional tracking detectors. The ability to stably deliver such a low-current calibration beam for similar tracking measurements

has been demonstrated in Hall C for the Qweak experiment, which similarly relies on using a tracking system for background and kinematics measurements, at a beam current 6 orders of magnitude lower than used for the primary asymmetry data-taking.

The tracking system will be used to verify the expected ratio of Møller to e-p distributions in both r and ϕ , to look for backgrounds from collimator punch-through and scraping, to study neutral backgrounds (by running in anti-coincidence with the main detectors), and, along with a PID system, to determine the π and μ backgrounds.

The utility of such a fast tracking system for studying backgrounds has recently been demonstrated in the commissioning of the Qweak experiment, where the “Region 3” vertical drift chamber system has been useful in understanding and limiting soft backgrounds in the Qweak main detectors.

In addition, we anticipate that the tracking system will prove useful for initial “tuneup” of the magnetic optics of the spectrometer. Comparison of the measured track distributions with simulated results as a function of magnetic field and target (liquid hydrogen, gaseous hydrogen, various solid targets) will be an essential way to “benchmark” the simulation and to verify spectrometer operation.

D.1.2 Effective Kinematics

The central value of Q^2 , weighted by acceptance and detector response, must be determined to 0.5% for this experiment. In principle, Q^2 can largely be determined from survey measurements of the collimator apertures and knowledge of the target location and length, along with the standard Hall A beam energy measurement (“Arc-energy”). The detectors should cover the full acceptance of events that pass through the collimators, so, to first order, precise measurement of their locations should not dominate the Q^2 determination. However, their analog response will come into play: in an integrating experiment such as this, the relative weight of a detected event in the asymmetry is determined by the amount of light detected at the PMT. If this analog response varies with Q^2 , it will skew the effective Q^2 distribution, and modify the central Q^2 . In the Qweak experiment, the effect on the central value of Q^2 is 2.5%. For that measurement, measuring this effect, and monitoring it during the course of the experiment, was one of the main motivations for their tracking system. While we don’t yet have a simulated estimate for this effect on this experiment (this awaits detailed detector design), we anticipate that it may be significant here as well. Mapping out and monitoring this analog response will be a major goal of the tracking system.

In addition, the large amount of multiple scattering, dE/dx and radiative losses due to the thick target, coupled with the large kinematic acceptance, and the rapid variation of the asymmetry with Q^2 , means that the Monte Carlo simulation of the effective Q^2 seen by each detector segment needs to be validated carefully. Again,

a tracking system with high spatial and angular resolution will be critical for this validation.

D.1.3 Conceptual Design

The present concept is that the tracking system will be located after the second toroidal magnet; it will measure the positions and angles of the tracks emerging from that magnet. Unlike the Qweak tracking system, we do not plan on having tracking elements located before the spectrometer magnets. The system will be removable for the primary asymmetry measurement, but will be periodically moved into place for tracking measurements. We are considering the use of two widely-separated planes of gas electron multiplier (GEM) chambers located in the evacuated drift region, followed by a final plane (in air) of either GEMs or straw-tube chambers, positioned just upstream of the main detector array. We are considering the possibility of a “Roman Pot” [8] arrangement for mounting the first two planes of GEMs, however we note that GEMs have been used under vacuum successfully [9].

D.1.4 Focal Plane Scanner

Another useful diagnostic will be a simple, small, movable detector that can operate at both the full beam flux and at the low beam currents needed for the tracking measurements. This “focal plane scanner” would consist of a small single Cerenkov detector made of fused silica, read out by PMTs, mounted on an x, y motion stage covering one sector of the acceptance, and located just upstream of the main detectors. Such scanners have been used in E158, HAPPEX-II, and one is now being used by Qweak. This device can be used to confirm that the rate distribution as measured at low beam currents by the full tracking system is not significantly different than that seen at full luminosity. It also would allow periodic rapid monitoring of the distribution during production data-taking, to ensure stability of the effective kinematics and to signal any changes in backgrounds.

Bibliography

- [1] Y. Li, F. Petriello and S. Quackenbush, Phys. Rev. D **80**, 055018 (2009) [arXiv:0906.4132 [hep-ph]].
- [2] W. F. Chang, J. N. Ng and J. M. S. Wu, Phys. Rev. D **79**, 055016 (2009) [arXiv:0901.0613 [hep-ph]].
- [3] Link for MOLLER Director's Review Report:
[http://hallaweb.jlab.org/12GeV/Moller/meetings/2010Aug31/Final Draft MOLLER Review Report.pdf](http://hallaweb.jlab.org/12GeV/Moller/meetings/2010Aug31/Final%20Draft%20MOLLER%20Review%20Report.pdf).
- [4] Link for MOLLER Director's Review Presentation Slides:
<http://hallaweb.jlab.org/12GeV/Moller/review/index.html>
- [5] I. Cohen *et al.*, Phys. Rev. Lett. **40**, 1614 (1978).
- [6] M. Alekseev *et al.*, Eur. Phys. J. **C64**, 171 (2009).
- [7] A. Boyarski *et al.*, Phys. Rev. **D14**, 1733 (1976).
- [8] P. Gutierrez, C. Hodges, K. Morgan and D. Schinzel, Nucl. Instrum. Methods **248**, 354 (1986).
- [9] J. Bossler, K. Gnanvo, J. Spanggaard, G. Tranquille, Proc. 9th European Particle Accelerator Conference (EPAC 2004), preprint: CERN-AB-2004-089.